FULL RESEARCH ARTICLE

CrossMark

A comparative study of microstructure and high-temperature mechanical properties of 15-5 PH stainless steel processed via additive manufacturing and traditional manufacturing

Dallas Roberts[1] · **Yi Zhang**[2] · **Indrajit Charit**[1] · **Jing Zhang**[2]

Abstract

In the present study, 15-5 PH Stainless Steel (SS) was produced via an additive manufacturing (AM) technique known as Direct Metal Laser Sintering (DMLS). The microstructure and mechanical properties of the AM alloy were compared with those of a traditionally manufactured (TM) or wrought 15-5 PH SS. Microstructural examination of both materials is performed by optical microscopy, transmission electron microscopy, and electron backscatter diffraction in a scanning electron microscope. A distinct difference was observed between the martensitic structure of the AM and TM alloys with the AM material with smaller grain sizes and round-shaped particles. The Vickers microhardness of the AM material was found to be greater than that of the TM material. Tensile testing at 593 °C exhibited a greater strength for the AM material compared to the TM material. Furthermore, the creep rupture life of the AM material was found to be greater compared to the TM material when tested at a temperature 593 °C and applied stress of 211 MPa. Fractographic examination of the crept and tensile specimens was conducted via scanning electron microscopy.

Keywords Additive manufacturing · Direct metal laser sintering · 15-5 PH stainless steel · Creep · Tensile testing · Microhardness

1 Introduction

Additive manufacturing (AM) is a relatively new, rapidly growing field with great potential to shape nearly all levels of manufacturing. AM has been broadly defined to cover any method of manufacturing parts from 3D model data, building products layer upon layer, rather than removing material to shape a blank to required specifications (i.e., subtractive manufacturing) [1, 2]. From its roots in polymer-based rapid prototyping developed in the late 1980s and early 1990s, to recent use in the production of complicated metal parts unable to be manufactured traditionally, AM promises to change global logistics, increase manufacturing energy efficiency, and reduce environmental impact [1, 2]. Although AM shows such promise, there are several hurdles to surmount before true large-scale, versatile industrial applications of the technique becomes successful. One of the primary issues is the lack of an AM materials property database [1]. The investigation of materials for use in AM machines and the development of said database of alloys have mostly focused on Ti-6Al-4V, even though recently more metallic alloys have been investigated [1]. One such alloy class is the precipitation hardenable stainless steels (SS) with the majority of the research work being focused on 17-4 PH SS [3–6]. However, a variant of 17-4 PH SS, 15-5 PH SS, is the material studied in this work. The material is used in multiple industries, including the aerospace, chemical, and food processing industries owing to its good combination of high strength, good corrosion resistance, good transverse toughness, and good forgeability [2]. However, studies on AM 15-5 PH SS have been quite limited [7–9].

Multiple AM techniques have been developed over the last couple of decades, and one of those techniques, Direct Metal Laser Sintering (DMLS), has been applied to 15-5 PH SS in the present study. DMLS is another name coined for

✉ Indrajit Charit
icharit@uidaho.edu

1   Department of Chemical and Materials Engineering,
    University of Idaho, Moscow, ID 83844-1021, USA

2   Department of Mechanical Engineering, Indiana
    University-Purdue University Indianapolis, Indianapolis,
    IN 46202-5191, USA

Selective Laser Sintering (SLS) to differentiate processes involving metal powders from those involving polymer powders, due to differing laser wavelengths used [10, 11]. The majority of DMLS machines are fed via powder bed, with a work area that is covered with powder via a rake, which is then sintered by the heat created by the laser into the desired geometry under an inert atmosphere [1]. In fact, it is a special category under the laser powder bed fusion (PBF) process and involves partial melting. Advantages of this system include a high resolution for features, an ability to create internal passages, and good-dimensional control [1]. However, care must be taken to ensure the parameters of the laser which are well adjusted to deliver the appropriate energy density to the feed powder. If the energy density is too low, incomplete sintering of the powder layer will occur, whereas too high an energy density could cause inhomogeneities via uneven melting, or vaporization of materials if the powder decomposition energy is reached [10, 11].

Interestingly, only a few studies on DMLS manufactured steel of this type are found in the open literature [7–9]. Moreover, to the best of authors' knowledge, high-temperature mechanical property data of these AM materials are not available, which are critically needed for high-temperature application of the material. The current study constitutes a preliminary investigation on microstructural characteristics, microhardness, and high-temperature mechanical property data of this AM 15-5 PH SS in comparison to the traditionally manufactured (TM) or wrought material. The mechanical data are also supplemented with microstructural and fractographic results.

2 Experimental

The AM samples were prepared by an EOSINT M270 (EOS GmbH Electro Optical Systems, Germany) machine equipped with a 200 W single mode Yb fiber laser with a wavelength of 1070 nm. Processing parameters were as follows: laser power of 170 W, a scanning speed of 1250 mm/s in continuous wavelength mode, a spot size of approximately 50 μm, hatch spacing of 100 μm, and a layer thickness of 30 μm. Processing was carried out under an argon environment to prevent oxidation.

The feed powder used was EOS Stainless Steel PH1, a 15-5 PH powder that conforms to standard 15-5 PH chemistry, nominal composition of which is Fe (balance), Cr (14–15.5 wt%), Ni (3.5–5.5 wt%), Cu (2.5–4.5 wt%), Mn (max. 1 wt%), Si (max. 1 wt%), Mo (max. 0.5 wt%), Nb (0.15–0.45 wt%), and C (max. 0.07 wt%). The AM samples were printed into cylindrical rods with 15 mm diameter × 90 mm length for later sectioning. Following DMLS, only a low-temperature stress-relieving heat treatment was applied to the printed parts, which was not enough to alter

microstructure or mechanical properties. TM (i.e., wrought) 15-5 PH SS round bars were procured from the marketplace as cylindrical bar stock of 25 mm diameter. Unfortunately, the exact processing conditions are not known.

Room-temperature density measurement of both samples was performed following the Archimedean principle. This was done to ensure that the density of the TM and AM materials is comparable. Density of both the materials was found to be about 7.8 g/cm^3.

Both tensile and creep specimens were machined from the above-mentioned cylindrical rods/bars of TM and AM materials along the longitudinal direction. Both creep and tensile specimens were kept cylindrical, and the gauge length and gauge diameter were 25.4 and 6.4 mm, respectively. Creep tests on both TM and AM specimens were carried out in an ATS Series 2320 MM Lever Arm Creep Tester at 593 °C and 211 MPa. Tensile tests were carried out using an Instron 5982 testing system at 593 °C with a strain rate of 10^{-3} s^{-1}. One AM specimen was tested at room temperature at a strain rate of 10^{-3} s^{-1}. The strain was calculated from the rate of cross-head movement and hence elastic moduli of the samples could not be determined from the tensile tests. Due to a lack of enough samples, only one sample of each type was available for these tests.

Samples for microhardness and TEM were sectioned using via diamond wafering blade, and hot mounted in black phenolic mounting powder with a Pace Technologies Mounting Press at 170 °C. These samples were then ground from 250 to 1200 grit and polished to a final surface finish of 1 μm. Next, the metallographic samples were etched with Aqua Regia (3 part hydrochloric acid and 1 part nitric acid, by volume).

Vickers microhardness tests were carried out on the samples, one from each cross section (transverse and longitudinal) of the TM and AM materials, using a Leco LM100 Microhardness Tester with a load of 0.5 kg$_f$ with a standard dwell time of 15 s. For each sample face, 17 indentations were made.

Metal sections from both AM and TM materials were thinned below 100 μm, punched into 3-mm diameter disks, and jet polished using an electrolyte of composition 15 vol% nitric acid and 85 vol% methanol in a Fischione twin-jet electropolisher at about −35 °C. They are examined using a JEOL 2010J TEM at an accelerating voltage of 200 kV.

Scanning electron microscopy was performed to examine the fracture surfaces of the AM-creep and tensile samples under secondary electron imaging mode in a Zeiss Supra 35 Scanning Electron Microscope (SEM) at an accelerating voltage of 10 kV. Electron backscatter diffraction (EBSD) studies were undertaken in the same SEM using a Quasor Electron Backscatter Diffraction system controlled by Fisher ThermoScientific NSS software. An accelerating voltage of 20 kV on the high current setting was used to capture the

data, and a pixel binning of 4×4 was used to minimize noise and information loss. Samples for EBSD were prepared in the same way as the TEM samples, with less time spent to prevent the formation of a hole during electro-jet polishing. The preparation method was adequate for creating the damage-free surface condition for the EBSD studies.

3 Results and discussion

3.1 Microstructural examination

The microstructural characterization was performed using optical microscopy. Figure 1a shows an optical micrograph of the TM 15-5 PH SS in the transverse cross-section. On the other hand, Fig. 1b shows an optical micrograph taken

from the longitudinal cross-section. The microstructures in two perpendicular sections appear quite similar and mainly consist of martensitic structure. It is worth noting that examination of the as-polished surfaces of the AM metallographic samples did not reveal any pores.

However, optical microscopy could not resolve the microstructure of the AM material and appear to be quite different from the TM material even at higher magnification (500×). Figure 2a, b shows the microstructure of the AM material in the transverse and longitudinal cross-sections, respectively. It appears that the martensitic structure in the AM material is much finer than the TM material.

However, the optical microscopy examination did not reveal any fine microstructural details. It necessitated further investigation into the microstructure using characterization tools such as TEM and EBSD. A bright-field TEM
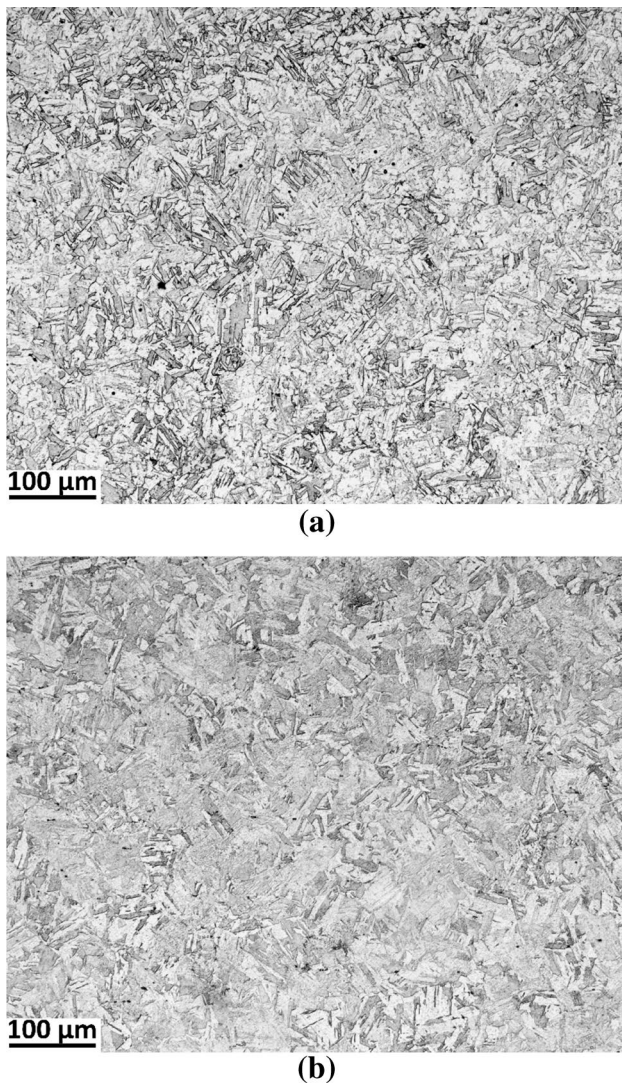

(a)

(b)

Fig. 1 Optical micrographs of the TM 15-5 PH SS samples in the **a** transverse and **b** longitudinal cross-sections
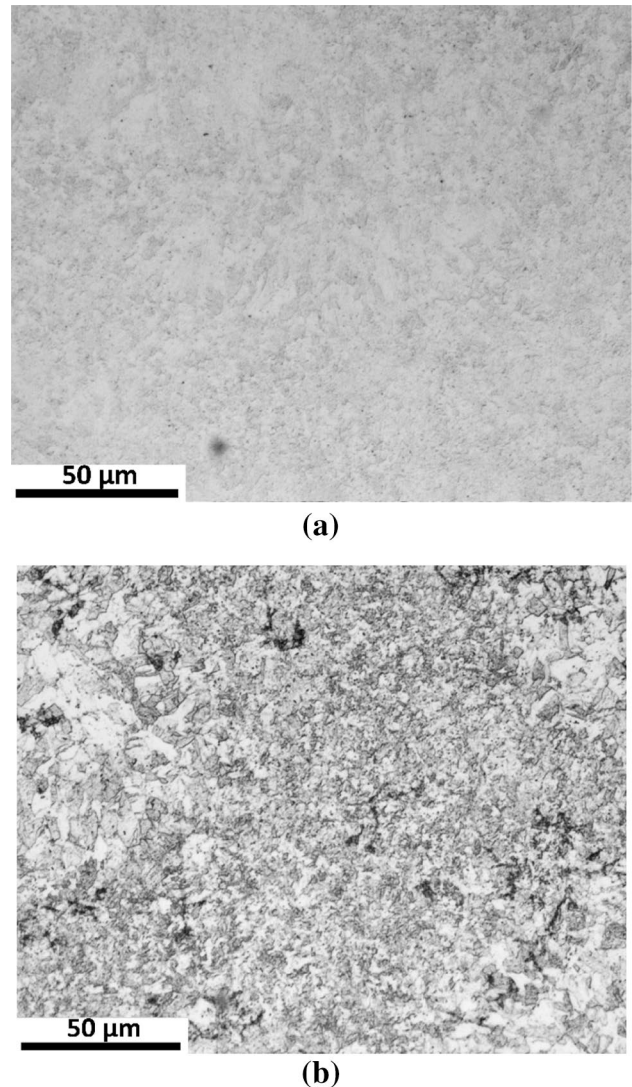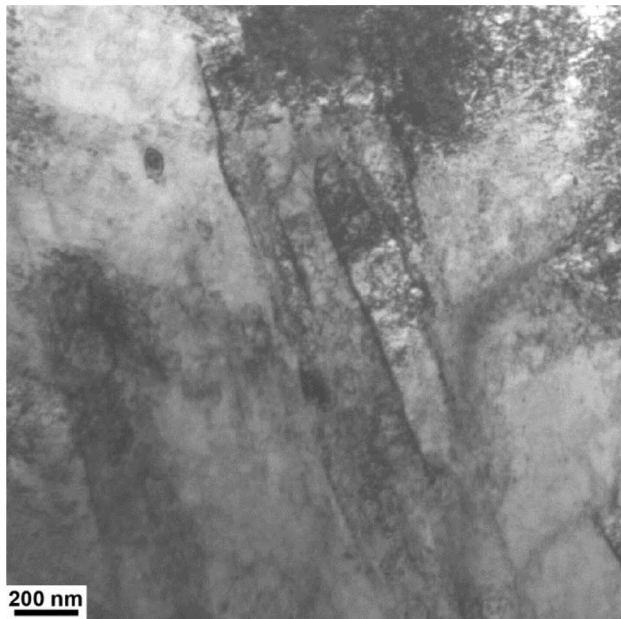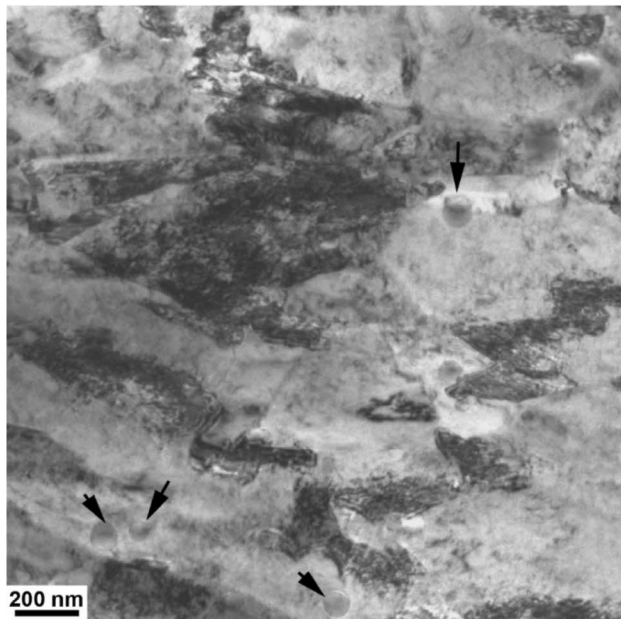

(a)

(b)

Fig. 2 Optical micrographs of the AM 15-5 PH samples in the **a** transverse and **b** longitudinal cross-sections

(a)

(b)

Fig. 3 Bright-field TEM images of **a** TM and **b** AM 15-5 PH stainless steel

image of the TM 15-5 PH steel is shown in Fig. 3a. Some martensitic elongated, 100–200 nm-wide lath structures can be observed. However, other regions of the TM sample did not have consistent lath features. Figure 3b shows a TEM micrograph of the AM 15-5 PH steel sample. No elongated lath features are observed; rather, short packets of narrower lath structures are visible. The microstructure is found to contain high dislocation density. Both specimens appear to
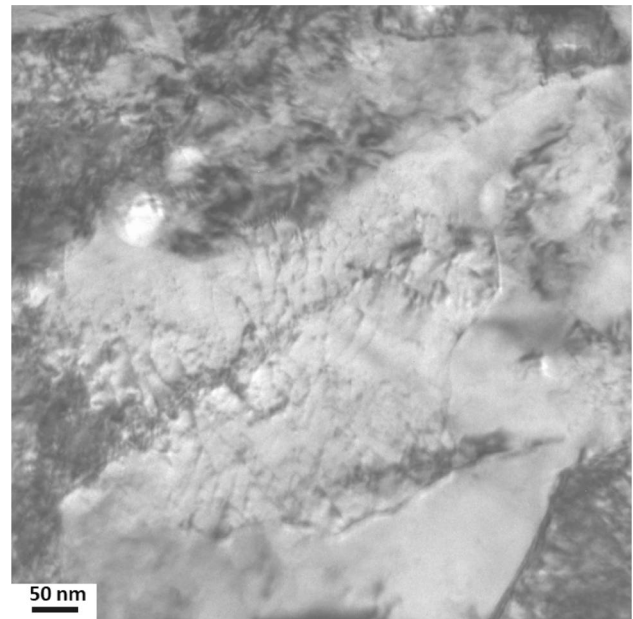

Fig. 4 Bright-field TEM image showing interactions of dislocations with nanometric precipitates in AM 15-5 PH SS

contain dislocations and identification of fine particles was difficult because of mottled contrast of the microstructure. One interesting observation was that the AM material contains several spherical particles of 70–90 nm in diameter (some of them shown by arrows in Fig. 3b), which were not be observed in the TM material. At this point, their chemical identity is not known and further investigation is ongoing.

Figure 4 shows that a high-magnification TEM image of the AM sample show dislocation activity. It appears that there many nanometric particles which could not be resolved clearly can be seen interacting with dislocations. These could be the coherent copper precipitates. In fact, copper precipitates are expected as 15-5 PH steel contains a maximum of 4.5 wt% copper.

Figure 5a, b shows the inverse pole figure maps of the TM and AM 15-5 PH SS. Both TM and AM samples show predominantly elongated grains, with TM lath sizes larger than the AM ones. Figure 6 shows the grain boundary misorientation distributions of the TM and AM samples. The TM sample has aligned grains with most grains having less than 10° misorientation. In comparison, a portion of grain boundaries (about 7%) in the AM sample has a larger misorientation around 30°.
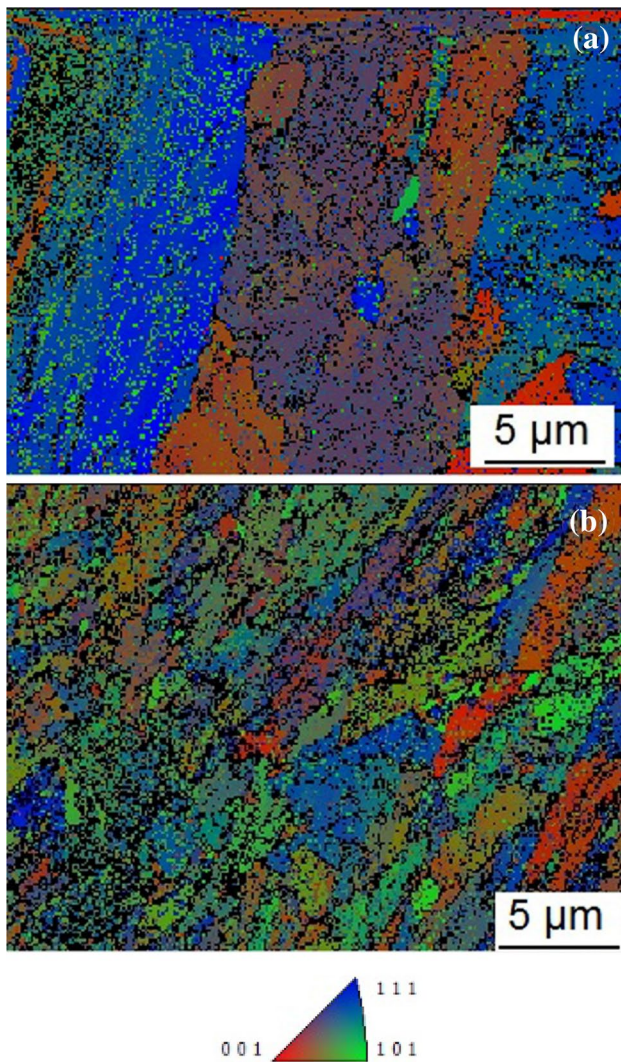
Fig. 5 Inverse pole figure maps (along the axis of the rod) of **a** TM and **b** AM 15-5 PH SS materials. Note that both maps show the distribution of other phases. The overlaid dark spots on the BCC map generated are possibly related to phases such as niobium carbide and other particles that could not be indexed

3.2 Mechanical properties

3.2.1 Microhardness testing

Vickers microhardness tests were performed on the transverse and longitudinal cross-sections of both TM and AM samples. The microhardness data are summarized in Table 1. The TM material has a lower hardness than the AM material. Furthermore, the hardness data confirm that the AM material is much harder than the TM material.

3.2.2 Tensile properties

Uniaxial tensile tests were conducted on both the TM and AM materials at a temperature of 593 °C and a strain rate of 10^{-3} s^{-1}. Figure 7 shows the engineering stress–engineering strain curves of the TM and AM materials. Tensile properties such as yield strength, ultimate tensile strength, and percentage elongation to fracture are listed in Table 2. The yield strength and ultimate tensile strength values are found to be close in both TM and AM materials, which demonstrates quite limited strain hardening capability in both these materials. However, the AM material has almost 30% higher yield strength and 32% higher ultimate tensile strength than the TM material; however, the percentage elongation to fracture and reduction in area (measures of ductility) is found to be relatively low in the AM material compared to the TM material. Room-temperature tensile testing at a strain rate of 10^{-3} s^{-1} of AM 15-5 PH SS resulted in yield strength of 850 MPa, ultimate tensile strength of 940 MPa, and elongation to fracture of 10%. The room-temperature data of the TM 15-5 PH SS used in the present study could not be evaluated because of the limited sample availability. The ASM handbook states that the wrought 15-5 PH SS has yield strength of 1170 MPa, ultimate tensile strength of 1310 MPa, and elongation to fracture of 10% [12]. However, the handbook provides an average data without mentioning which heat treatment. At higher temperature (i.e., 593 °C), the AM material exhibits only a 7% reduction in yield strength, and a 12% reduction in ultimate tensile strength, while the TM material exhibited 49 and 53% reductions to these parameters, respectively. Thus, it is evident that the microstructural features helped the AM material to better retain strength at the elevated temperature than the TM material.

3.2.3 Comparison of creep properties

In this study, creep rupture tests on the TM and AM specimens were conducted at a temperature of 593 °C under an applied stress of 211 MPa. Figure 8 shows the corresponding creep curves of the TM and AM materials. Given the short span of these creep tests, they can be basically termed well as stress rupture tests. The creep curves do not exhibit any clear primary and steady-state stages presumably because of the high-temperature and high-stress level employed during these creep tests. The rupture life for the AM material was found to be 157.2 h as opposed to that of 121.2 h for the TM material. Accordingly, the minimum creep rate for the AM material is measured to be 0.0003%/h and the TM material to be 0.038%/h. In a wrought and annealed 15-5 PH SS, the minimum creep rate was measured to be 0.015%/h [13]. Under the creep test conditions, it can be noted that the AM material has superior creep properties compared to the
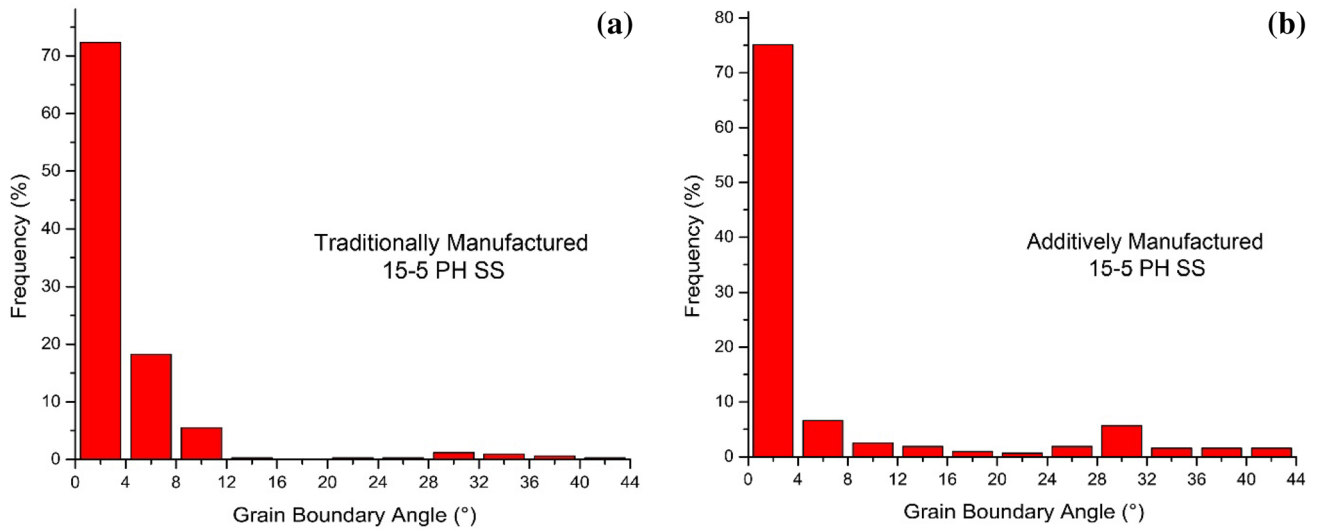
Fig. 6 Grain boundary misorientation histograms for **a** TM and **b** AM 15-5 PH SS

Table 1 Vickers microhardness data of 15-5 PH SS under the TM and AM conditions

	Traditional 15-5 PH		Additively manufactured 15-5 PH	
	Transverse	Longitudinal	Transverse	Longitudinal
Vickers Microhardness (HV$_{0.5}$)	320 ± 14	330 ± 8	500 ± 12	460 ± 10

Table 2 Summary of tensile properties of the TM and AM 15-5 PH SS at 593 °C and a strain rate of 10^{-3} s^{-1}

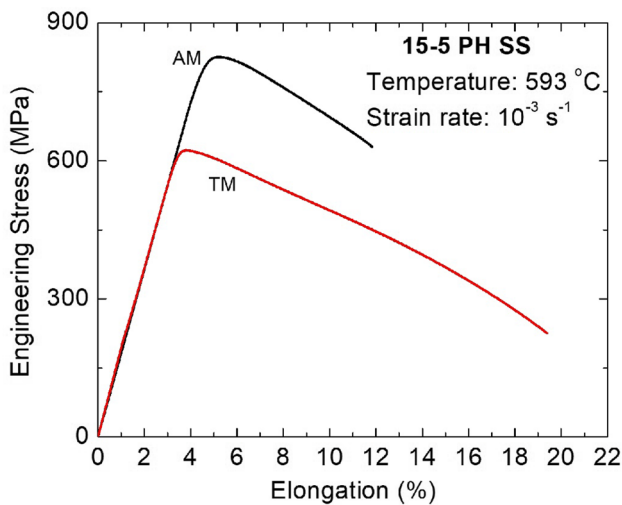| Tensile property	TM	AM
Yield strength (MPa)	610	790
Ultimate tensile strength (MPa)	620	830
Elongation to fracture (%)	19	9
Reduction in area (%)	70	50

Fig. 7 Engineering stress–engineering strain curve for 15-5 PH SS of the traditionally manufactured (TM) and additively manufactured (AM) 15-5 PH SS
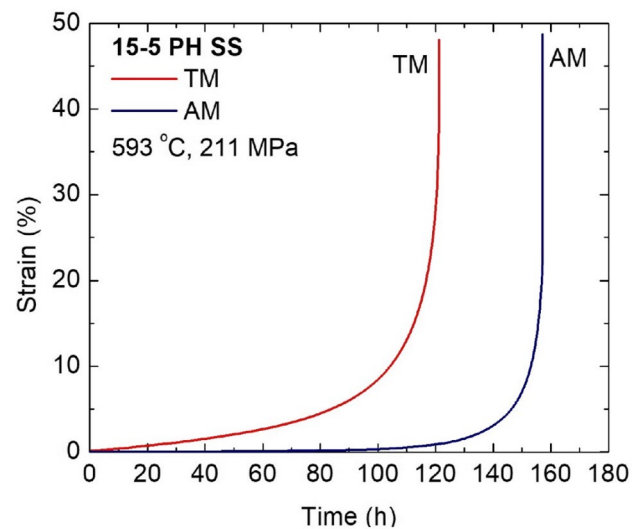

Fig. 8 Creep curves of TM and AM 15-5 PH SS (test conditions: temperature of 593 °C and applied stress of 211 MPa)

TM material. More creep tests need to be conducted to fully understand the unique creep behavior of the AM materials.

3.2.4 Fractographic examination

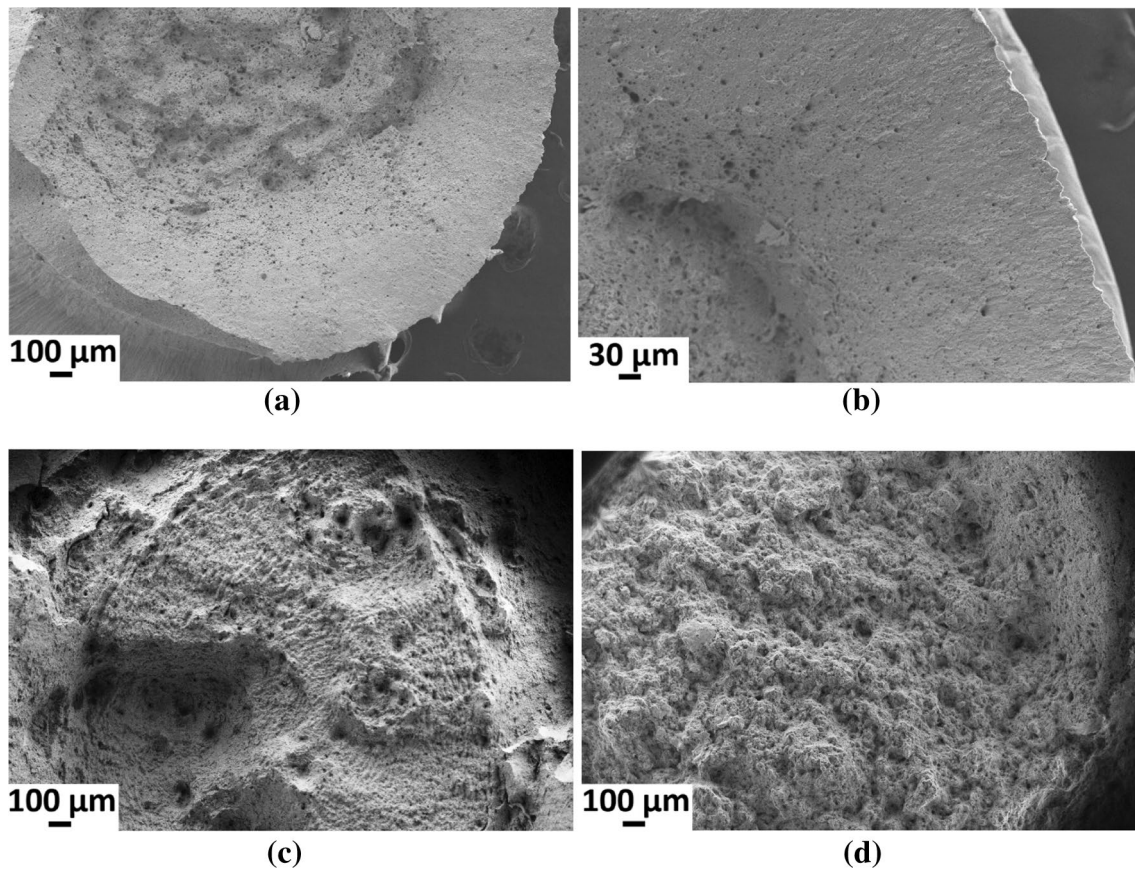Scanning electron microscopy was performed on the fracture

Fig. 9 SEM secondary electron images of the fracture surfaces of the following 15-5 PH SS specimens tested at 593 °C: **a** TM-tensile testing; **b** TM-creep testing; **c** AM-tensile testing; **d** AM-creep testing

surfaces of both tensile and creep specimens of the AM and TM materials. The purpose of the SEM fractographic study was to examine whether there is any evidence of difference in tensile and creep failure behavior. Figure 9a, b shows the fracture surfaces of tensile and creep specimens of the TM 15-5 PH SS, respectively. The fracture surfaces in the tested tensile and creep specimens did not reveal any major difference in dimple morphology. The overall roughness of the dimpled surface did not have any special features.

The fracture surface of the AM-tensile-tested specimen is shown in Fig. 9c, while the AM-creep-tested specimen is shown in Fig. 9d. The AM-tensile-tested specimen exhibits some interesting features. The surface structure appears to contain wavy, layer-like structure. However, the width of the wave-like features is 25–30 μm. This is probably associated with the size of the powder layers which were used to build the AM rod. Note that the layer size used was about 30 μm as reported in the "Experimental" section. As we have seen before, the martensite lath structure was about 100–200 nm, so these layers which are much wider than the martensitic laths do not correspond

to the features observed on the fracture surface. However, the fracture surface examined for the creep tested AM 15-5 PH SS sample revealed surface topography quite different from the tensile-tested AM sample, wherein the wave-like structures are not apparent any more. Greater time at the elevated temperature and low strain rate may have provided opportunities for the material to plastically flow differently influencing the failure mode and creating quasi-dimple features.

4 Conclusions

The present study reported some interesting results on the microstructure and mechanical properties of the 15-5 PH SS that was made via AM process (DMLS) in comparison with a TM (wrought) 15-5 PH SS. Microstructural examination of both materials revealed martensitic microstructure. The microstructure of the AM material could not be revealed well by optical microscopy given its fineness. The TEM and EBSD studies revealed somewhat different lath

structures with much shorter and narrower laths present in the AM material compared to the TM material. Some characteristic round-shaped particles were also detected in the AM material.

The Vickers microhardness of the AM material at room temperature was found to be greater (by approximately 50%) than that of the TM material. Tensile tests at 593 °C exhibited a greater strength (by about 30%) for the AM material compared to the TM material, while the AM material had a lower ductility (by more than 50%). Furthermore, the creep life of the AM material was found to be greater compared to the TM material when tested at 593 °C and 211 MPa. At the closing, it can be unequivocally said that the preliminary results obtained from the AM material is quite promising. However, further testing and relevant microstructural analyses need to be conducted to fully understand the high-temperature mechanical behavior of the AM material.

Compliance with ethical standards

Conflict of interest On behalf of all authors, the corresponding author states that there is no conflict of interest.

References

1. Frazier W (2014) Metal additive manufacturing: a review. J Mater Eng Perform 23(6):1917–1928
2. Murr LE, Gaytan SM, Ramirez DA, Martinez E, Hernandez J, Amato KN, Shindo PW, Medina FR, Wicker RB (2012) Metal fabrication by additive manufacturing using laser and electron beam melting technologies. J Mater Sci Technol 28(1):1–14
3. Rafi HK, Pal D, Patil N, Starr TL, Stucker B (2014) Microstructure and mechanical behavior of 17-4 precipitation hardenable steel processed by selective laser melting. J Mater Eng Perform 23:4421–4428
4. Facchini L, Vincente N, Lonardelli I, Magalini E, Robotti P, Molinari A (2010) Metastable austenite in 17–4 precipitation-hardening stainless steel produced by selective laser melting. Adv Eng Mater 12(3):184–188
5. LeBraun T, Nakamoto T, Horikawa K, Kobayashi H (2015) Effect of retained austenite on subsequent thermal processing and resultant mechanical properties of selective laser melted 17-4 PH stainless steel. Mater Des 81:44–53
6. AlMangour B, Yang J-M (2017) Understanding the deformation behavior of 17-4 precipitate hardenable stainless steel produced by direct metal laser sintering. Int J Adv Manuf Technol 90:119–126
7. Spierings AB, Starr TL, Wegener K (2013) Fatigue performance of additive manufactured metallic parts. Rapid Protyp J 19(2):88–94
8. Rafi HK, Starr TL, Stucker BE (2013) A comparison of tensile, fatigue and fracture behavior of Ti-6Al-4V and 15-5 PH Stainless Steel parts made by selective laser melting. Int J Adv Manuf Technol 69(5–8):1299–1309
9. Buchanan C, Matilainen V-P, Salminen A, Gardner L (2017) Structural performance of additive manufactured metallic materials. J Construc Steel Res 136:35–48
10. Lee H, Lim CHJ, Low MJ, Tham N, Murukeshan VM, Kim YJ (2017) Lasers in additive manufacturing: a review. Int J Precision Eng Manuf 4(3):307–322
11. Khaing MW, Fuh JYH, Lu L (2001) Direct metal laser sintering for rapid tooling: processing and characterization of EOS parts. J Mater Process Technol 113:269–272
12. ASM Handbook (1993) Volume 1: properties and selection: irons, steels, and high-performance alloys 1993, ASM International, Materials Park
13. Deel OL, Mindlin H (1972) Engineering Data on New Aerospace Structural Materials, Technical Report, AFML-TR-71-196

Publisher's Note Springer Nature remains neutral with regard to jurisdictional claims in published maps and institutional affiliations.